Sensors and Actuators Reports 3 (2021) 100059

Contents lists available at ScienceDirect

Sensors and Actuators Reports

journal homepage: www.sciencedirect.com/journal/sensors-and-actuators-reports

Water enabled self-healing polymeric coating with reduced graphene oxide-reinforcement for sensors

Kally C.S. Ly [a], Mawin J.M. Jimenez [a], Silvia Cucatti [a], Diogo Volpati [b], Marcelo A. Pereira-da-Silva [c,d], Flavio M. Shimizu [a], Tiago P. Almeida [a,e], Varlei Rodrigues [a], Jose Alberto F. da Silva [f], Fernando Alvarez [a], Antonio Riul Jr [a,*]

[a] Department of Applied Physics, "Gleb Wataghin" Institute of Physics (IFGW), University of Campinas (UNICAMP), 13083-970, Campinas, SP, Brazil
[b] Division of Solid State Physics and NanoLund. Lund University, Lund 221 00, Sweden
[c] Instituto de Física de São Carlos – IFSC/USP, 13560-250, São Carlos, SP, Brazil
[d] Centro Universitário Central Paulista - UNICEP, São Carlos, SP,Brasil
[e] Department of Biotechnology, Delft University of Technology, Van der Maasweg 9, 2629 HZ Delft, the Netherlands
[f] Department of Analytical Chemistry, Chemistry Institute, University of Campinas (UNICAMP), 13083-970, Campinas, SP, Brazil

ARTICLE INFO

Keywords:
Self-healing
Multifunctional coating
Layer-by-layer
Reduced graphene oxide
Hardness

ABSTRACT

Intrinsic self-healing materials have received significant attention due to the characteristic recovery after damage properties through reversible dynamic covalent and non-covalent interactions. Furthermore, functional recovery with reliable mechanical properties are highly keen as protective coatings, specifically for devices and sensors vulnerable to abrasion in severe environments. Here, we present a functional hierarchical nanostructure capable of multiple micro-sized healings, with enhanced mechanical hardness due to the incorporation of graphene oxide (rGO) nanoplatelets. A self-healing multilayered nanocomposite formed by poly(ethylene imine) (PEI) and poly (acrylic acid) (PAA) was easily assembled by the layer-by-layer (LbL) technique. The addition of the rGO nanoplatelets in the LbL nanostructure resulted in a 13-fold increase in hardness (0.4 ± 0.1 GPa) when compared to the (PEI/PAA) architecture (0.03 ± 0.01 GPa). In addition, the nanocomposite presents an enhanced insulating electrical behavior ($\sim 4.10^{-8}$ S/cm) despite the addition of the rGO nanoplatelets. Raman and Zeta Potential analysis indicated a possible wrapping of the rGOs by PEI, justifying the observed insulating electrical characteristics. The nanocomposite presents good hydrophobicity with a water contact angle of 136°, interesting to extend the lifetime and protect underlying layers from humidity, degradation, and encrustation. Therefore, we propose an attractive hydrophobic, electrically insulating, and mechanically resistant multifunctional coating for high-performance electronic interfaces from minor cuts and abrasions, dispensing maintainer intervention.

1. Introduction

Nature-inspired, and first defined by Scott R. White, self-healing materials can restore properties/functions after mechanical damage by using available inner resources [1]. They are tailored to increase lifetime and reduce waste, degradation, maintenance, and costs of devices, with potential application in protective coatings [2–4], health-monitoring systems [5–8], and flexible electronics [9–11]. Briefly, extrinsic self-healing materials need an integrated healing agent (microcapsules, nanocapsules embedded in a polymeric matrix) to restore the damaged area, being unable of multiple regenerations at the same damaged region [12–14]. Intrinsic self-healing materials are mainly based on reversible dynamic covalent and non-covalent interactions, without healing agents to perform the regeneration process, although sometimes it may require external stimuli such as water, heat, or light [13,15]. Nowadays, the ultimate goal is the development of multifunctional coatings having high durability even in severe environments, which may demand, for example, efficient control of mechanical resistance, healing ability, and wettability of the coating.

Within this framework, the LbL technique provides an elegant, facile way to design and fabricate hierarchical nanostructures with well-defined thickness, composition, and structure, regardless the substrate morphology [16–19]. In the LbL assembly the intrinsic self-healing occurs with the migration of molecules from the deposited layers to the

* Corresponding author.
E-mail address: riul@ifi.unicamp.br (A. Riul).

https://doi.org/10.1016/j.snr.2021.100059
Received 24 August 2021; Received in revised form 27 September 2021; Accepted 14 October 2021
Available online 29 October 2021

damaged area [20,21]. Wang et al. [22] demonstrated that a high pH difference between oppositely charged polyelectrolytes leads to a better healing ability of the LbL structures. Qi et al. [23] fabricated a quasi-linear LbL self-healing film made of poly(vinyl alcohol) (PVA), tannic acid (TA), and graphene oxide (GO) in a (PVA-GO/TA) structure having an epidermis-like morphology and a tooth enamel hardness, with the healing mechanism based on hydrogen bonding and electrostatic interactions. Zhu et al. [24] reported the preparation of graphene-reinforced self-healing LbL films having improved electrochemical performance. Fan et al. [25] incorporated GO with branched poly(ethyleneimine) (bPEI)/poly(acrylic acid) (PAA) multilayers to improve the corrosion resistance of interfaces. Overall, a general challenge for polymeric self-healing materials is to overcome the vulnerability to abrasion by increasing the mechanical resistance of the self-repairing coatings. However, the healability decreases with increasing loading of materials used to elevate the mechanical resistance of interfaces [26].

Here, we present a reinforced composite incorporating functionalized rGOs nanoplatelets (NPLs) in a PEI/PAA LbL self-healing matrix. The rGO NPLs were functionalized with poly(allylamine hydrochloride) (PAH) or poly(sodium 4-styrenesulfonate) (PSS), thus forming rGO nanoplatelets wrapped by PAH or PSS molecules. rGO NPLs wrapped by PAH are named here as GPAH, analogically for GPSS. Previous studies on GPAH and GPSS report non-covalent intermolecular bonding interactions between rGO and the polymers, preserving good chemical stability, mechanical stiffness, and electrical conductivity [27–32]. However, the formed $(GPAH\text{-}PEI/GPSS\text{-}PAA)_n$ nanocomposite presented conductivity values ($\sim 4.10^{-8}$ S/cm) four times lower than that observed for $(PEI/PAA)_{60}$. Raman and Zeta Potential analysis indicated a physical interaction between GPAH and PEI molecules, thus hampering electric conduction pathways between rGO nanoplatelets in the composite LbL film. We also observed a water contact angle of 136°, a hydrophobicity that can be favorably used in the protection from humidity, degradation, and fouling. If in contact with water, this multifunctional LbL assembly can quickly recover from damages within 15 min, together with better mechanical hardness of the composite. Its high electrical resistivity can also be further explored to tailor the electrical anisotropy of multilayered nanostructures in FET devices [33].

2. Material and methods

2.1. Materials

Poly(acrylic acid) ($M_w \sim 8000$, 45 wt.% in H_2O), poly(ethylene imine) ($M_w \sim 2000$), poly(allylamine hydrochloride) ($M_w \sim 250{,}000$, 35 wt.% in H2O), poly(sodium 4-styrenesulfonate) ($M_w \sim 200{,}000$, 30 wt.% in H_2O) and graphene oxide (GO) are acquired from Sigma-Aldrich. GO is then chemically reduced to rGO and functionalized with PSS or PAH molecules similarly to literature [27], thus forming, respectively, GPSS and GPAH. All solutions are prepared with deionized water acquired from a Sartorius Arium Comfort system.

2.2. LbL film

A homemade setup automatically controlled by Arduino is used to fabricate the LbL structures [34]. Glass slides are previously cleaned with ammonium hydroxide, hydrogen peroxide and water (1:1:5 v/v/v) at ~ 80 °C for 10 min. A mixture of PEI (4 mg/mL) + GPAH (0.1 mg/mL), (1:1 v/v) at pH = 10.5 is used as the positive polyelectrolyte, and PAA (4 mg/mL) + GPSS (0.1 mg/mL), (1:1 v/v) at pH = 3.0 is used as the negative polyelectrolyte (Fig. 1a). When necessary, the pH is adjusted by adding 1 M solutions of HCl or NaOH. Briefly, a cleaned glass slide is immersed 15 min [24,35] in the positive polyelectrolyte and then washed in ultrapure water at pH = 10.5 to remove the excess of material loosely bound. In the sequence, the glass slide is immersed 15 min in the negative polyelectrolyte, followed by another washing step in ultrapure water at pH = 3.0 (Fig. 1b), thus forming $(GPAH\text{-}PEI/GPSS\text{-}PAA)_n$ LbL films as illustrated in Fig. 1. $(GPAH/GPSS)_{50}$ and $(PEI/PAA)_{60}$ LbL films are used as control experiments, with all assembly parameters listed in Table 1.

2.3. Analyses

Zeta Potential experiments are performed on GPAH and GPSS solutions to investigate the electrical charge of the polyelectrolytes in a broad pH range, using a Zetasizer Nano ZS ZEN 36,000 (Malvern Instruments). The LbL films are analyzed by Raman Spectroscopy with a Micro Raman XploRA from Horiba Scientific using a 532 nm laser excitation source and a 100X objective. The scattered light is dispersed with an 1800/mm grating through a 10% filter, with an exposure time of 8 s and 8 accumulations. Atomic Force Microscopy (AFM)

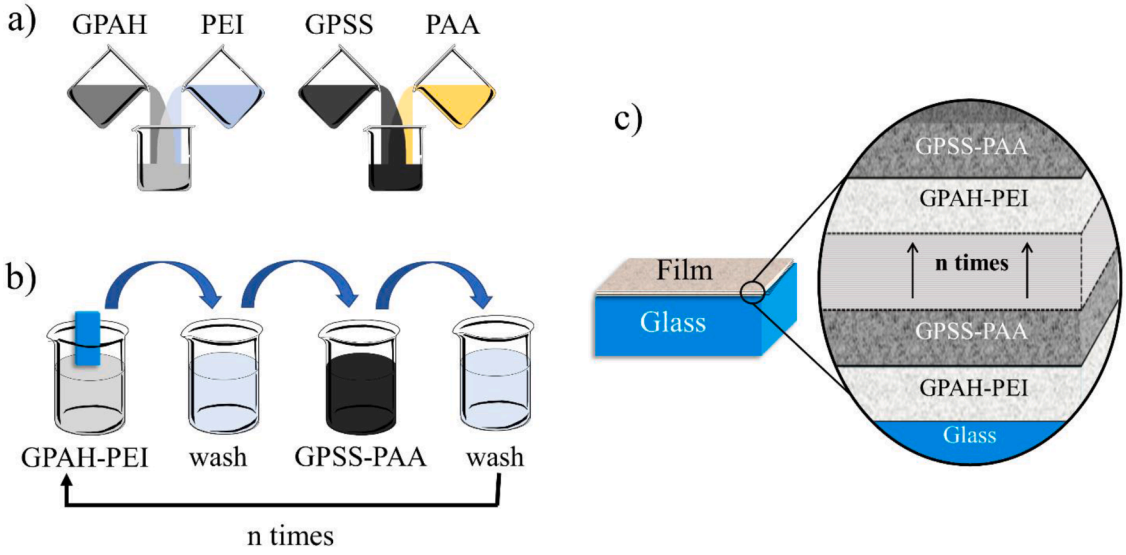

Fig. 1. LbL film fabrication. (a) Preparation of the polyelectrolytes mixing GPAH with PEI, and GPSS with PAA, both (1:1) in volume; (b) Fabrication of the multilayered LbL nanostructure, and (c) Schematic illustration of the $(GPAH\text{-}PEI/GPSS\text{-}PAA)_n$ LbL film.

Table 1
LbL nanostructures assembled in this work, with the parameters used for the film formation.

LbL architecture	material	Concentration (mg/mL)	pH	Immersion Time (min)
(GPAH-PEI/GPSS-PAA)$_{60}$	GPAH	0.1	10.5	15
	PEI	4		
	GPSS	0.1	3.0	15
	PAA	4		
(PEI/PAA)$_{60}$	PEI	4	10.5	15
	PAA	4	3.0	15
(GPAH/GPSS)$_{50}$	GPAH	0.1	3.5	10
	GPSS	0.1	3.5	10

measurements are taken on a Bruker Dimension ICON equipment with a rectangular-shaped silicon tip set to intermittent contact mode, with 42 N/*m* spring constant and 330 kHz free oscillation. The healing ability of the LbL films is checked with a Dino Lite USB microscope AM7515MT4A. A profilometer Dektak 150 is used to determine quantitatively the depth of the mechanical damage made in the films with an STM tip. Once the scratch is healed, the image is registered with the film dried at ambient conditions. The wettability of the films is analyzed with an optical tensiometer DSA 100 Standard and software Drop Shape Analyzer from Krüss. The hardness of the LbL nanostructures is investigated using a NanoTest, Berkovich diamond indenter from Micro Materials. For hardness data analysis it is adopted the Oliver-Pharr model [36]. Nanoindentation depths are fixed at 500 nm, corresponding to less than 20% of the estimated film thickness. Current (I) vs voltage (V) measurements are acquired at each deposition step of LbL films deposited on gold interdigitated electrodes (IDEs) having 30 pairs of fingers with 150 nm height, 3 mm of length (L), 40 μm width (W) and separated 40 μm from each other (L). The (I - V) curves are obtained coupling the homemade automated LbL setup controlled by Arduino with a Keithley 6487 Picoammeter [34].

3. Results and discussion

3.1. Component analyses

Fig. 2 illustrates the Zeta potentials for GPAH and GPSS solutions. The PAH response prevails for GPAH solutions, as the allylamine hydrochloride group is positively charged bellow pH 9 and presents an isoelectric point around pH 9 [37]. On the other hand, GPSS keeps a negative zeta potential in the whole pH range studied, as PSS is a strong and not pH dependent polyanion [38]. The literature indicates that the best pH for the LbL film fabrication are, respectively, pH ~ 10 for PEI and 3 < pH < 5 for PAA [22,25]. That led us to prepare the polyelectrolytes as follows: (PEI + GPAH) aqueous solutions at pH = 10, and (PAA + GPSS) aqueous solutions at pH = 3.5. It is worth mentioning the stability of the GPAH and GPSS (± 40 mV) aqueous suspensions [27–29], with the literature indicating a tendency of PEI become deprotonated around pH ~ 10 [39–42], which may interfere on the molecular vibration of the GPAH-PEI mixture. In addition, this method represents a non-covalent approach based on supramolecular complexation using PEI (PAA) to wrap GPAH (GPSS) nanoplatelets, i.e., the driving force between polymers and rGO can be van der Waals forces, π−π interactions, and hydrogen bonding, as will be discussed in the Raman section.

Raman spectra of the (GPAH-PEI/GPSS-PAA)$_{60}$, (GPAH/GPSS)$_{50}$, and (PEI/PAA)$_{60}$ LbL films are illustrated in Fig. 3, with the last one used for comparison and better comprehension of the composite system. It is observed the characteristic vibrational bands of graphene at 1583 cm^{-1} (G-band) due to the sp^2 bond stretching of atoms in both rings and chains, and at 1343 cm^{-1} (D-band) attributed to defects of the rGO nanoplatelets owing to the breathing modes of sp^2 atoms in rings [43]. The I_D/I_G ratio for (GPAH/GPSS)$_{50}$ is 1.1, in good agreement with the literature[20,27,28] where the increase of the I_D/I_G ratio also indicates a successful transformation of GO in rGO together with a degradation of the overall size of the formed sp^2 domains [44]. Regarding the polymers, it is noticed in (PEI/PAA)$_{60}$ bands at 1106 cm^{-1} due to the stretching of the C—COO$^-$ groups from PAA molecules and at 1560 cm^{-1} due to the

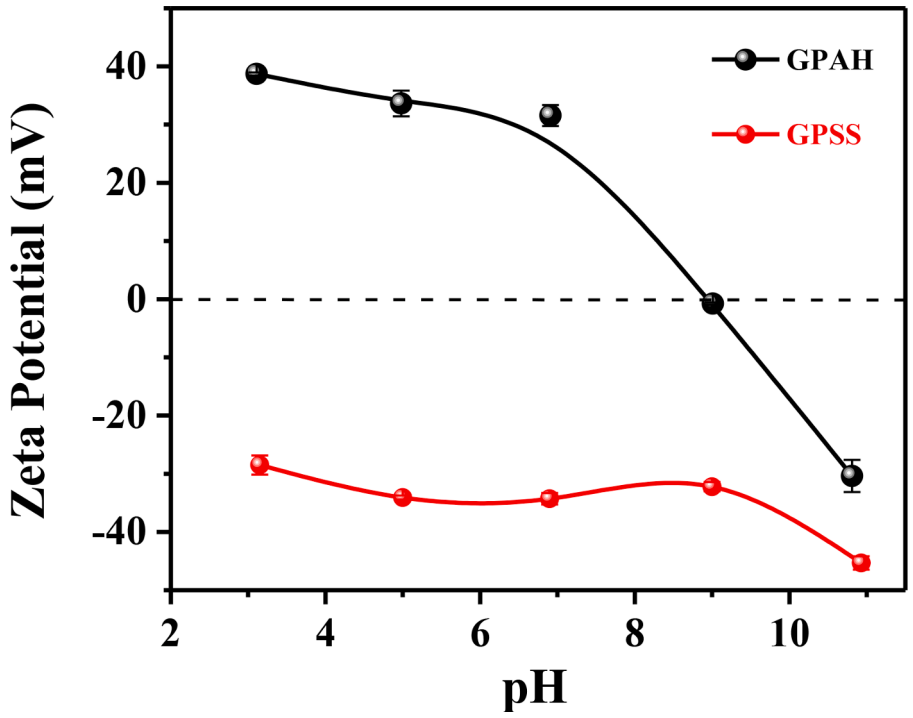

Fig. 2. Zeta potential measurements. Zeta potential for GPAH (black line) and GPSS (red line) solutions prepared in different pH. Some error bars are too small to be observed.

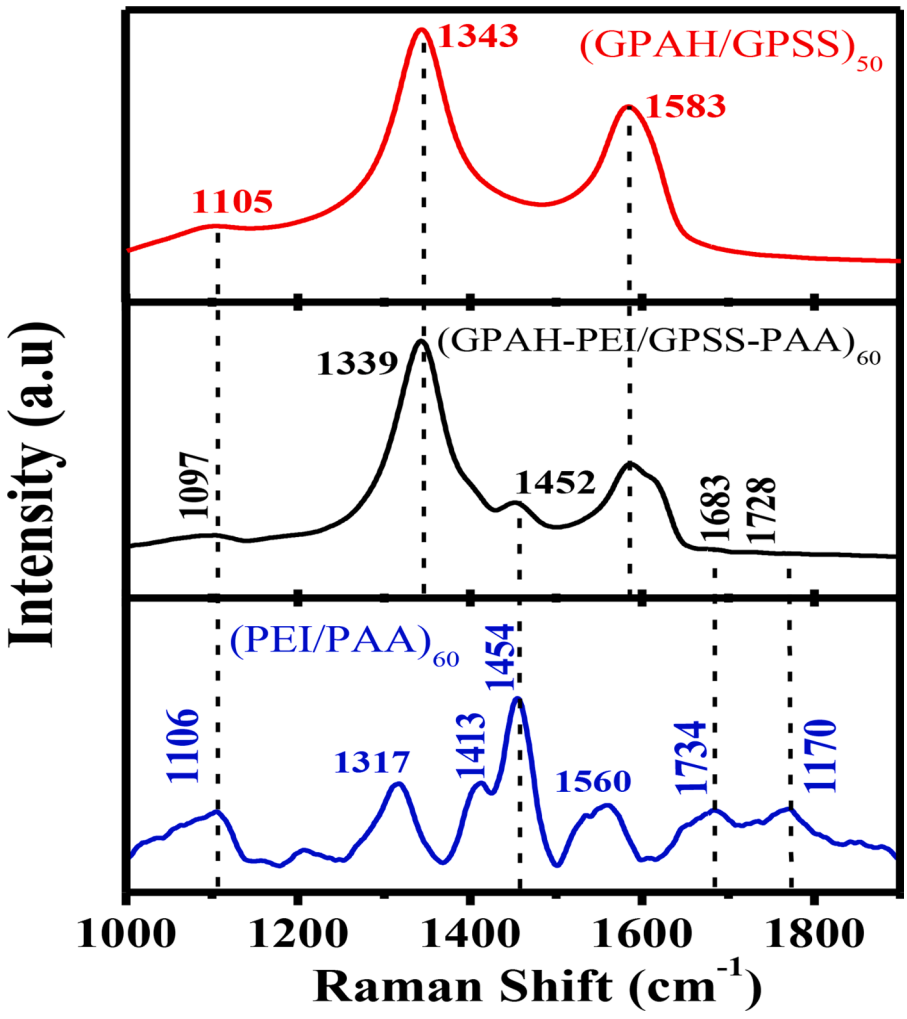

Fig. 3. Raman spectra. Raman spectra of $(GPAH\text{-}PEI/GPSS\text{-}PAA)_{60}$, $(GPAH/GPSS)_{50}$ and $(PEI/PAA)_{60}$ LbL films.

N—H bending vibration of NH_2 groups from PEI [45]. The composite $(GPAH\text{-}PEI/GPSS\text{-}PAA)_{60}$ spectrum presents the main bands from both $(GPAH/GPSS)_{50}$ and $(PEI/PAA)_{60}$, thus indicating that the $(GPAH\text{-}PEI/GPSS\text{-}PAA)_{60}$ LbL film is a hybrid system preserving the main molecular vibrations discussed above. It is worth mentioning the decrease of the G band intensity at 1583 cm^{-1} in the $(GPAH\text{-}PEI/GPSS\text{-}PAA)_{60}$ LbL film compared to $(GPAH/GPSS)_{50}$, and also the non-appearance of an expected vibrational peak at 1560 cm^{-1} from PEI, suggesting an electrostatic interaction between PEI and GPAH. Such hypothesis agrees with the previous Zeta Potential analysis and others arguments in the literature [39–42], once the NH_2 group from PEI may be deprotonated at the pH value used here. Therefore, our results suggest the wrapping of the GPAH nanoplatelets by PEI molecules in solution before the LbL assembly and van der Waals forces as a driving interaction between PEI (PAA) molecules and GPAH(GPSS).

3.2. Electrical analyses

The electrical properties illustrated in Fig. 4 derive from the wrapping in solution between PEI and GPAH nanoplatelets. Consequently, a low electrical conduction is observed for the $(GPAH\text{-}PEI/GPSS\text{-}PAA)_{60}$ film, considering the separation of rGO conducting islands in the composite LbL structure. It is a direct evidence of physical interactions between GPAH and PEI as discussed above, with the conductivity of $(GPAH/GPSS)_{50}$ ($\sim 1.10^{-4}$ S/cm) orders of magnitude higher than that measured for $(GPAH\text{-}PEI/GPSS\text{-}PAA)_{60}$ ($\sim 4.10^{-8}$ S/cm) and $(PEI/PAA)_{60}$ ($\sim 2.10^{-7}$ S/cm). The electrical characteristics of $(GPAH/GPSS)_{50}$, $(GPAH\text{-}PEI/GPSS\text{-}PAA)_{60}$ and $(PEI/PAA)_{60}$ structures (Fig. 4) are calculated from the I-V curves acquired during the LbL assembly [27]:

$$\sigma_{dc} = (R.K_{cell})^{-1} \quad (1)$$

where K_{cell} is the cell constant of the IDEs. A simplified equation can be obtained for K_{cell} when $L = W$:

$$K_{cell} = (N-1)L/2 \quad (2)$$

$(GPAH/GPSS)_{50}$ displays a current orders of magnitude higher than $(PEI/PAA)_{60}$ and $(GPAH\text{-}PEI/GPSS\text{-}PAA)_{60}$ (Fig. 4), with a thermally activated hopping conduction [27]. Although we initially expected higher conduction for $(GPAH\text{-}PEI/GPSS\text{-}PAA)_{60}$ due to the increase of rGO nanoplatelets dispersed in the polymeric matrix, the composite $(GPAH\text{-}PEI/GPSS\text{-}PAA)_{60}$ film presented a conductivity 4 times lower than that observed for $(PEI/PAA)_{60}$. This result corroborates both Raman and Zeta Potential analyses indicating a physical interaction between GPAH and PEI molecules, which hinders conductive pathways in the LbL film structure, resulting in the observed high resistive in-plane electrical behavior. This is particularly interesting to control electric anisotropy in multilayered structures for field-effect or flexible electronic devices. One final remark on the blue curve in the inset at −1 V and 1 V is that it is ruled by the presence of water molecules trapped in the LbL structure, as previously reported in [20].

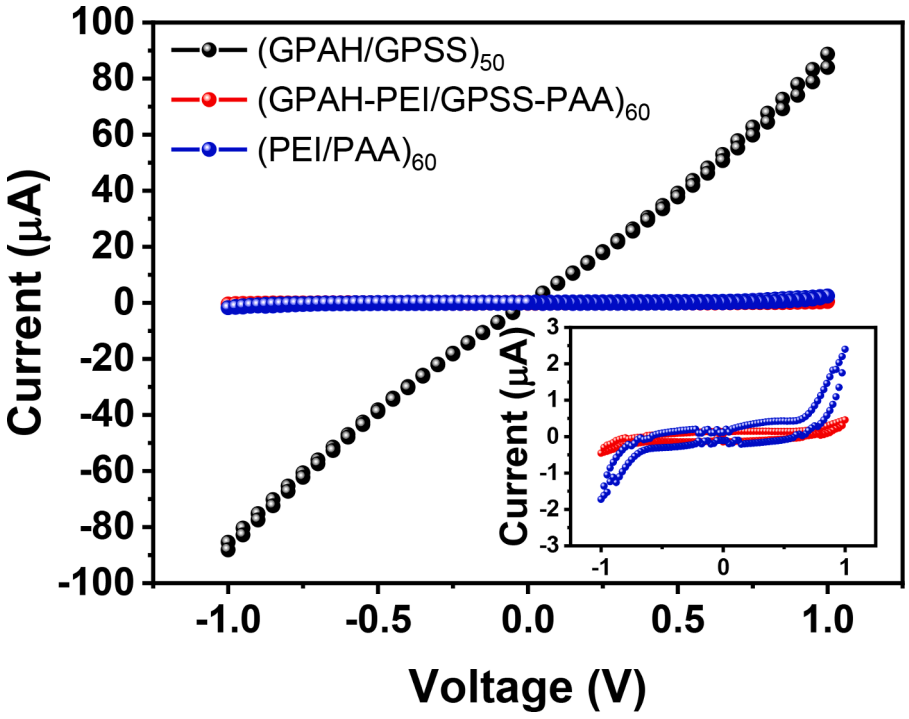

Fig. 4. Electrical analyses. I-V measurements from −1 V to 1 V for $(PEI/PAA)_{60}$, $(GPAH/GPSS)_{50}$ and $(GPAH\text{-}PEI/GPSS\text{-}PAA)_{60}$ LbL films. Inset: Zoom at the low current region.

3.3. Healability and hydrophobicity tests

The healing ability of the nanocomposite is checked through cuts having tens of microns that were completed restored after immersing the damaged area 15 min. in water, illustrated in Fig. 5. The results are in the average healing efficiency (recovery time, cut depth) values reported for (PEI/PAA) LbL films in the literature. Table 2 brings the detailed information of similar works for reference and comparison [22,25,46,47]. It is often observed in the literature an increase in hardness with the addition of other materials in a self-healing matrix, which can seriously compromise the healing performance. Here, we have successfully maintained the self-healing capability of the LbL composites, as the optimized rGO reinforcement did not bring significant changes to the healing process of scratched coatings when compared to PEI/PAA films.

What happens in the studied coating is that the positive GPAH-PEI composite interacts with the negative GPSS-PAA part by electrostatic forces. The water stimulus causes the swelling effect that saturates after a certain time, thus favoring higher mobility to the polymer chains that migrate to the damaged region separated by micrometers of distance. As the rGO nanoplatelets are isolated in the polymer matrix and also present in smaller quantities, it is expected that they do not interfere with

Table 2
Demonstration of the healability of several PEI/PAA based self-healing films in literature and in this work.

Structure	Immersion time	Cut dimensions	Ref.
PEI/PAA	5 min	50 μm	[22]
Ce(IV)/GO/PEI/PAA	10 min	10 μm	[25]
MoS_2/(PAA-AD/PEI-β-CD)	30 min	20 μm	[46]
PAA-AD/PEI-β-CD	30 min	50 μm	[47]
GPAH-PEI/GPSS-PAA	15 min	10μm	this work

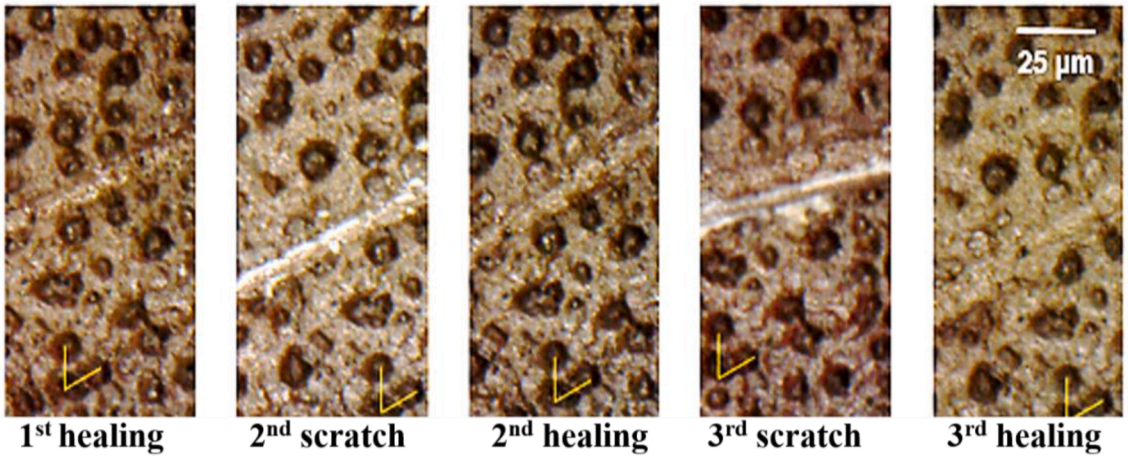

Fig. 5. Healability tests. $(GPAH\text{-}PEI/GPSS\text{-}PAA)_{60}$ fil scratched by a STM tip. The damaged area had ~ 10 μm width and 30 μm depth, followed by immersion in water for 15 min for the healing process. The yellow V mark at the bottom of Fig. 5 is a reference to prove that the damages occurred in the same region.

the swelling and healing processes, enriching only the mechanical properties of our films. The corresponding schematic is illustrated in Fig. 6.

The water contact angle (WCA) for the $(PEI/PAA)_{60}$ film is (130° ± 2°), with a slight increase observed in the $(GPAH\text{-}PEI/GPSS\text{-}PAA)_{60}$ structure (CA = 136° ± 5°), being both LbL assemblies hydrophobic. A comparative AFM analysis in a (2 × 2) μm^2 scanned area is performed (see in Support Information Figure S1), indicating differences in the surface roughness by AFM and profilometry analyses are distinct each other due to the dimension (1D vs. 2D) and extension (1.5 mm vs. 2 × 2 μm^2) of the scanned regions. A rougher surface is obtained with the addition of rGO nanoplatelets, resulting in average root mean square roughness values of 55 nm for $(GPAH\text{-}PEI/GPSS\text{-}PAA)_{60}$ film, 16 nm for $(GPAH/GPSS)_{50}$, and 13 nm for $(PEI/PAA)_{60}$. The higher surface roughness in $(GPAH\text{-}PEI/GPSS\text{-}PAA)_{60}$ is the reason for the increased WCA, resembling the hierarchical structure observed in nature [48–50]. The average thickness of the $(PEI/PAA)_{60}$ and $(GPAH/GPSS)_{50}$ films in a (2 × 2) μm^2 area are ~ 6 μm and ~100 nm, respectively. The thickness of $(GPAH\text{-}PEI/GPSS\text{-}PAA)_{60}$ film is measured by profilometry as the cut region presented a quite irregular surface for AFM analysis, with an average thickness of ~ 15 μm in a 1.5 mm measured profile line. The regeneration illustrated in Fig. 7 indicates an effective migration of the molecules to the damaged area, with the measured profile along with the healed scratch (~ 13 μm thick) comparable to the average surface roughness of the analyzed extension (~ 15 μm).

3.4. Hardness test

Fig. 8 illustrates the load-depth curve as a result of the hardness test by nanoindentation for both $(GPAH\text{-}PEI/GPSS\text{-}PAA)_{60}$ and $(PEI/PAA)_{60}$ structures. Up to the same depth profile it is necessary ten times more load for the $(GPAH\text{-}PEI/GPSS\text{-}PAA)_{60}$ structure, which quantitatively imply in a hardness (H) of (0.4 ± 0,1) GPa for the nanocomposite that is indeed 13 times higher than that presented by the $(PEI/PAA)_{60}$ film (H = (0.03 ± 0.01) GPa). Hummod et al. [51] also investigated the nanomechanical behavior of PEI/PAA film using nanoindentation, obtaining a hardness of H = (0.44 ± 0.06) GPa at similar humidity condition. It is worth mentioning that their films were deposited on silicon and ours on glass. Our system consists of a soft film deposited on a hard substrate, a case where the influence of the substrate on the hardness of the film should be negligible according to the literature [52]. What could be considered on the LbL film growth on different substrates is the influence of the substrate used in the formation of the first LbL layers, thus altering structural properties and influencing the film hardness.

Xiang et al. [26] fabricated a self-healing LbL film composed by PAA with branched PEI grafted with ferrocene (bPEI-Fc) and rGO nanosheets modified with βcyclodextrin (RGO—CD). The as-prepared PAA/bPEI-Fc & RGO—CD presented a hardness of 1.0 GPa, which is by far the highest hardness value of all reported self-healing LbL films in the literature. Experimental results showed that the mobility of the bPEI-Fc polyelectrolytes within the $(PAA/bPEI\text{-}Fc\&RGO\text{—}CD_{0.04})_{45}$ films is significantly suppressed by the rGO nanofillers due to their strong host−guest interactions. Consequently, the healability is no longer efficient in water being necessary the immersion of the LbL film in H_2O_2 solution, which increase processing steps, costs and may be eventually harmful depending on the application. However, in our work the polymeric wrapping of the rGO NPLs did not compromise the mobility of the materials in the healing process, enabling multiple regenerations of the composite $(GPAH\text{-}PEI/GPSS\text{-}PAA)_{60}$ structure with water addition at room temperature. Therefore, the $(GPAH\text{-}PEI/GPSS\text{-}PAA)_{60}$ structure also presented improved hardness when compared to (PEI/PAA), good hydrophobicity and electrical insulation.

4. Conclusions

We demonstrated an rGO reinforced coating that increases the mechanical hardness of LbL coatings without compromising the self-healing ability of the formed composite. Hierarchical multilayered nanostructures were easily prepared allowing functional films presenting multiple regenerations at the same damaged area after contact with water. The LbL $(GPAH\text{-}PEI/GPSS\text{-}PAA)_{60}$ composite also presented higher hydrophobicity, surface roughness, and electrical resistivity than $(PEI/PAA)_{60}$ due to the wrapping of GPAH nanoplatelets by PEI molecules in solution, previous to the LbL assembly deposition. It forms an attractive insulating LbL framework where minor cuts and abrasions are difficult and time-consuming to locate and repair, becoming a valuable tool to form new transistor architectures where the film can both act as a channel and insulating layer, paving the way for future field effect devices or organic electronics.

Associated content

Supporting information

I-V measurements and AFM analysis of the LbL films (file type: PDF)

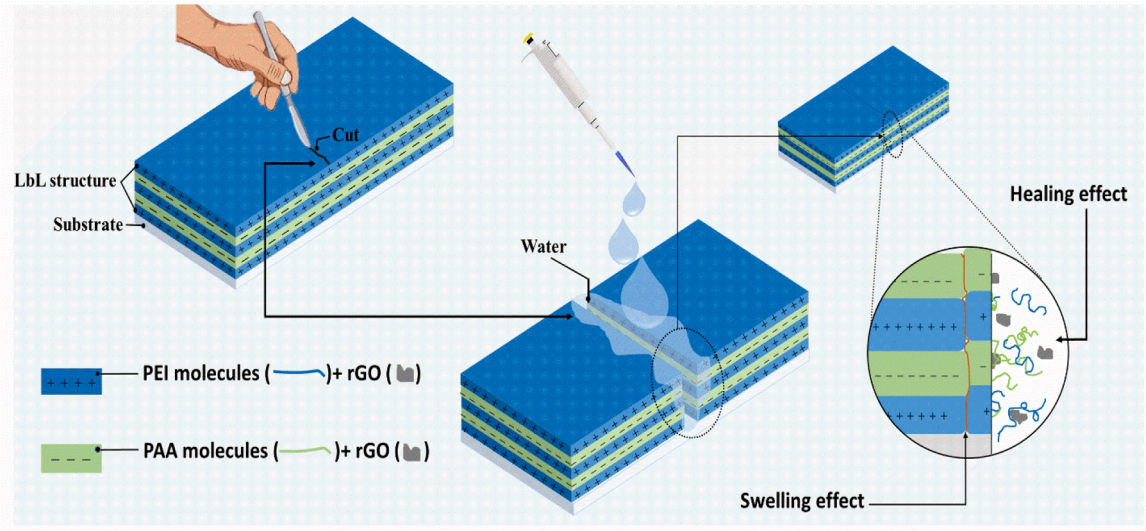

Fig. 6. Schematic diagram of the involving interactions of the self-healing process.

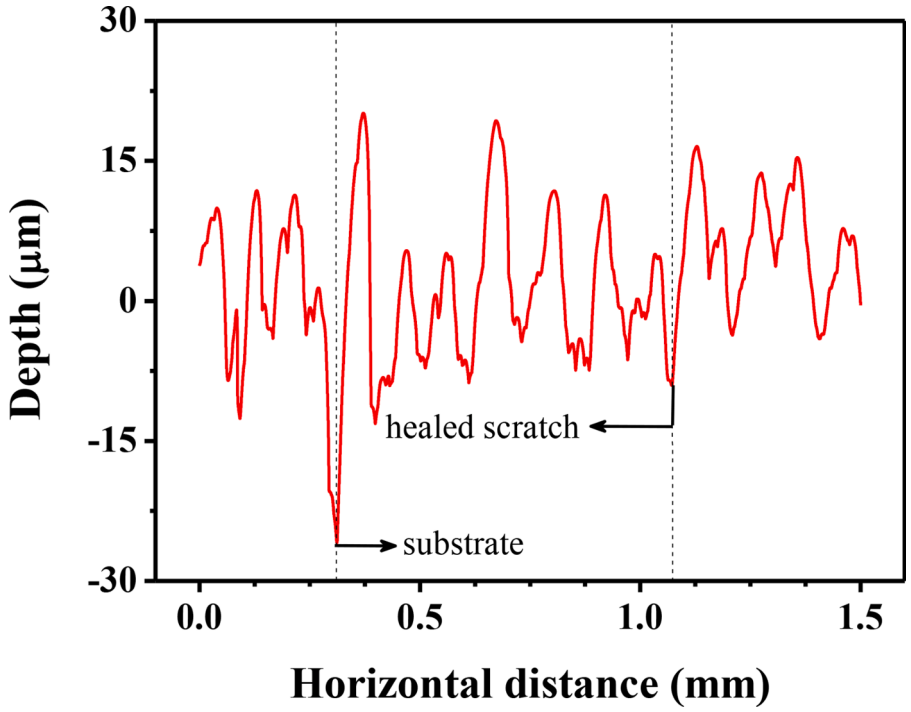

Fig. 7. Profilometry measurements of the (GPAH-PEI /GPSS-PAA)$_{60}$ film. The first depth demarcated by the left vertical line represents a scratch on the LbL film, with the second line on the right representing the healed area after damage occurred in the same region.

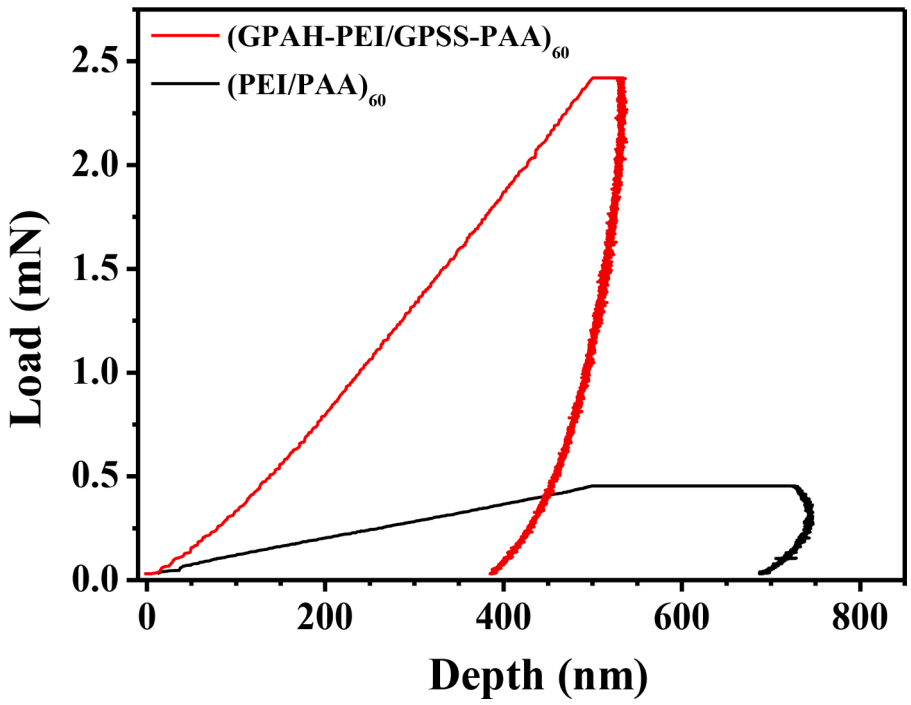

Fig. 8. Hardness tests. Load vs. depth obtained from the nanoindentation measurements for the films (PEI/PAA)$_{60}$ e (GPAH-PEI/GPSS-PAA)$_{60}$.

Funding

This work was supported by FAPESP (2014/03691-7), CAPES and National Council for Scientific and Technological Development – CNPq.

Declaration of Competing Interest

The authors declare no conflict of interest.

Acknowledgments

Authors are grateful for the financial support given by FAPESP (2014/03691-7), CAPES and National Council for Scientific and Technological Development – CNPq (407418/2018-0 and 303869/2018-6). They also thank Brazilian Nanotechnology National Laboratory (CNPEM) for the IDEs and Prof. Monica A. Cotta from the Department of Applied Physics, "*Gleb Wataghin*" Institute of Physics (IFGW - UNICAMP)

for lending the Keithley 6487 Picoammeter.

Supplementary materials

Supplementary material associated with this article can be found in the online version at doi:10.1016/j.snr.2021.100059.

References

[1] B.J. Blaiszik, S.L.B. Kramer, S.C. Olugebefola, J.S. Moore, N.R. Sottos, S.R. White, Self-Healing Polymers and Composites, Annu. Rev. Mater. Res. 40 (2010) 179–211, https://doi.org/10.1146/annurev-matsci-070909-104532.

[2] C. Zhou, J.T. Zhou, X.Q. Ma, D. Pranantyo, J.J. Li, L.Q. Xu, V.X. Truong, Robust anti-infective multilayer coatings with rapid self-healing property, Mater. Sci. Eng. C-Mater. Biol. Appl. 121 (2021) 11, https://doi.org/10.1016/j.msec.2020.111828.

[3] J. Zhang, J. Wei, B. Li, X. Zhao, J. Zhang, Long-term corrosion protection for magnesium alloy by two-layer self-healing superamphiphobic coatings based on shape memory polymers and attapulgite, J. Colloid Interface Sci. 594 (2021) 836–847, https://doi.org/10.1016/j.jcis.2021.03.005.

[4] M. Wang, H.X. Sun, F.R. Cao, W. Tian, L. Li, Moisture-triggered self-healing flexible perovskite photodetectors with excellent mechanical stability, Adv. Mater. 33 (2021) 8, https://doi.org/10.1002/adma.202100625.

[5] Y.X. Sun, W. Wang, Y. Sheng, R. Zhang, M. Bradley, Self-healing multilayer films for simultaneous release of hydrophilic and hydrophobic drugs, Soft Mater. 19 (2021) 254–262, https://doi.org/10.1080/1539445x.2020.1828099.

[6] C. Liu, L. Fan, Z. Tian, H. Wen, L. Zhou, P. Guan, Y. Luo, C. Chan, G. Tan, C. Ning, L. Rong, B. Liu, Self-curling electroconductive nerve dressing for enhancing peripheral nerve regeneration in diabetic rats, Bioact. Mater. 6 (2021) 3892–3903, https://doi.org/10.1016/j.bioactmat.2021.03.034.

[7] R.Q. Yuan, C.X. Luo, Y.F. Yang, C.P. He, Z.H. Lu, L.Q. Ge, Self-healing, high adherent, and antioxidative LbL multilayered film for enhanced cell adhesion, Adv. Mater. Interface. 7 (2020) 11, https://doi.org/10.1002/admi.201901873.

[8] W. Qiu, H. Han, M. Li, N. Li, Q. Wang, X. Qin, X. Wang, J. Yu, Y. Zhou, Y. Li, F. Li, D. Wu, Nanofibers reinforced injectable hydrogel with self-healing, antibacterial, and hemostatic properties for chronic wound healing, J. Colloid Interface Sci. 596 (2021) 312–323, https://doi.org/10.1016/j.jcis.2021.02.107.

[9] J. Xu, H. Wang, X. Du, X. Cheng, Z. Du, H. Wang, Highly stretchable PU ionogels with self-healing capability for a flexible thermoelectric generator, ACS Appl. Mater. Interface. 13 (2021) 20427–20434, https://doi.org/10.1021/acsami.1c03328.

[10] S. Liu, S. Chen, W. Shi, Z. Peng, K. Luo, S. Xing, J. Li, Z. Liu, L. Liu, Self-healing, robust, and stretchable electrode by direct printing on dynamic polyurea surface at slightly elevated temperature, Adv. Funct. Mater. (2021), https://doi.org/10.1002/adfm.202102225.

[11] J. Kang, J.B.H. Tok, Z. Bao, Self-healing soft electronics, Nat. Electron. 2 (2019) 144–150, https://doi.org/10.1038/s41928-019-0235-0.

[12] M.D. Hager, P. Greil, C. Leyens, S. van der Zwaag, U.S. Schubert, Self-healing materials, Adv. Mater. 22 (2010) 5424–5430, https://doi.org/10.1002/adma.201003036.

[13] Y.J. Tan, J. Wu, H. Li, B.C.K. Tee, Self-healing electronic materials for a smart and sustainable future, ACS Appl. Mater. Interface. 10 (2018) 15331–15345, https://doi.org/10.1021/acsami.7b19511.

[14] E. Kobina Sam, D. Kobina Sam, X. Lv, B. Liu, X. Xiao, S. Gong, W. Yu, J. Chen, J. Liu, Recent development in the fabrication of self-healing superhydrophobic surfaces, Chem. Eng. J. 373 (2019) 531–546, https://doi.org/10.1016/j.cej.2019.05.077.

[15] Z. Hu, Q. Shao, Y. Huang, L. Yu, D. Zhang, X. Xu, J. Lin, H. Liu, Z. Guo, Light triggered interfacial damage self-healing of poly(p-phenylene benzobisoxazole) fiber composites, Nanotechnology 29 (2018), 185602, https://doi.org/10.1088/1361-6528/aab010.

[16] G. Decher, Fuzzy nanoassemblies: toward layered polymeric multicomposites, Science 277 (1997) 1232–1237, https://doi.org/10.1126/science.277.5330.1232.

[17] R. Frisenda, E. Navarro-Moratalla, P. Gant, D. Perez De Lara, P. Jarillo-Herrero, R. V. Gorbachev, A. Castellanos-Gomez, Recent progress in the assembly of nanodevices and van der Waals heterostructures by deterministic placement of 2D materials, Chem. Soc. Rev. 47 (2018) 53–68, https://doi.org/10.1039/c7cs00556c.

[18] F.X. Xiao, M. Pagliaro, Y.J. Xu, B. Liu, Layer-by-layer assembly of versatile nanoarchitectures with diverse dimensionality: a new perspective for rational construction of multilayer assemblies, Chem. Soc. Rev. 45 (2016) 3088–3121, https://doi.org/10.1039/c5cs00781j.

[19] P. Bertrand, A. Jonas, A. Laschewsky, R. Legras, Ultrathin polymer coatings by complexation of polyelectrolytes at interfaces: suitable materials, structure and properties, Macromol. Rapid Commun. 21 (2000) 319–348, https://doi.org/10.1002/(sici)1521-3927(20000401)21:7<319::aid-marc319>3.0.co;2-7.

[20] G. Gaál, M.J.M. Jimenez, F. Alvarez, V. Rodrigues, A. Riul, Influence of water on electrical and mechanical properties of self-assembled and self-healing PEM films, Prog. Organ. Coat. 150 (2021), 105980, https://doi.org/10.1016/j.porgcoat.2020.105980.

[21] H. Chen, F. Cheng, C. Chen, H. Li, Study on self-healing behavior of the layer-by-layer assembled polyethylenimine/poly(acrylic acid) film, J. Appl. Polym. Sci. 137 (2020) 49169, https://doi.org/10.1002/app.49169.

[22] X. Wang, F. Liu, X. Zheng, J. Sun, Water-enabled self-healing of polyelectrolyte multilayer coatings, Angew. Chem. 50 (2011) 11378–11381, https://doi.org/10.1002/anie.201105822.

[23] X. Qi, D. Zhang, Z. Ma, W. Cao, Y. Hou, J. Zhu, Y. Gan, M. Yang, An epidermis-like hierarchical smart coating with a hardness of tooth enamel, ACS Nano 12 (2018) 1062–1073, https://doi.org/10.1021/acsnano.7b05478.

[24] Y. Zhu, C. Yao, J. Ren, C. Liu, L. Ge, Graphene improved electrochemical property in self-healing multilayer polyelectrolyte film, Colloid. Surf. A 465 (2015) 26–31, https://doi.org/10.1016/j.colsurfa.2014.10.035.

[25] F. Fan, C. Zhou, X. Wang, J. Szpunar, Layer-by-layer assembly of a self-healing anticorrosion coating on magnesium alloys, ACS Appl. Mater. Interface. 7 (2015) 27271–27278, https://doi.org/10.1021/acsami.5b08577.

[26] Z. Xiang, L. Zhang, Y. Li, T. Yuan, W. Zhang, J. Sun, Reduced graphene oxide-reinforced polymeric films with excellent mechanical robustness and rapid and highly efficient healing properties, ACS Nano 11 (2017) 7134–7141, https://doi.org/10.1021/acsnano.7b02970.

[27] M.J.M. Jimenez, R.F. Oliveira, T.P. Almeida, R.C.H. Ferreira, C.C.B. Bufon, V. Rodrigues, M.A. Pereira-da-Silva, A.L. Gobbi, M.H.O. Piazzetta, A. Riul, Charge carrier transport in defective reduced graphene oxide as quantum dots and nanoplatelets in multilayer films, Nanotechnology 28 (2017), 495711, https://doi.org/10.1088/1361-6528/aa91c2.

[28] A. Rani, K.A. Oh, H. Koo, H.j. Lee, M. Park, Multilayer films of cationic graphene-polyelectrolytes and anionic graphene-polyelectrolytes fabricated using layer-by-layer self-assembly, Appl. Surf. Sci. 257 (2011) 4982–4989, https://doi.org/10.1016/j.apsusc.2011.01.007.

[29] C.M. Miyazaki, M.A.E. Maria, D.D. Borges, C.F. Woellner, G. Brunetto, A. F. Fonseca, C.J.L. Constantino, M.A. Pereira-da-Silva, A. de Siervo, D.S. Galvao, A. Riul, Experimental and computational investigation of reduced graphene oxide nanoplatelets stabilized in poly(styrene sulfonate) sodium salt, J. Mater. Sci. 53 (2018) 10049–10058, https://doi.org/10.1007/s10853-018-2325-1.

[30] Y. Du, D. Li, L. Liu, G. Gai, Recent achievements of self-healing graphene/polymer composites, Polymers (Basel) (2018) 10, https://doi.org/10.3390/polym10020114.

[31] Y. Yue, N. Liu, Y. Ma, S. Wang, W. Liu, C. Luo, H. Zhang, F. Cheng, J. Rao, X. Hu, J. Su, Y. Gao, Highly Self-Healable 3D Microsupercapacitor with MXene-Graphene Composite Aerogel, ACS Nano 12 (2018) 4224–4232, https://doi.org/10.1021/acsnano.7b07528.

[32] G. Li, P. Xiao, S. Hou, Y. Huang, Graphene based self-healing materials, Carbon N Y 146 (2019) 371–387, https://doi.org/10.1016/j.carbon.2019.02.011.

[33] G. Gaál, M.L. Braunger, V. Rodrigues, A. Riul, H.L. Gomes, High electrical anisotropic multilayered self-assembled organic films based on graphene oxide and PEDOT:PSS, Adv. Electron. Mater. (2021), 2100255, https://doi.org/10.1002/aelm.202100255.

[34] R.C. Hensel, K.L. Rodrigues, V.d.L. Pimentel, A. Riul, V. Rodrigues, Automated self-assembly and electrical characterization of nanostructured films, MRS Commun. 8 (2018) 283–288, https://doi.org/10.1557/mrc.2018.47.

[35] Z. Xiang, L. Zhang, T. Yuan, Y. Li, J. Sun, Healability demonstrates enhanced shape-recovery of graphene-oxide-reinforced shape-memory polymeric films, ACS Appl. Mater Interface. 10 (2018) 2897–2906, https://doi.org/10.1021/acsami.7b14588.

[36] W.C. Oliver, G.M. Pharr, An improved technique for determining hardness and elastic modulus using load and displacement sensing indentation experiments, J. Mater. Res. 7 (1992) 1564–1583, https://doi.org/10.1557/jmr.1992.1564.

[37] H. Riegler, F. Essler, Polyelectrolytes. 2. Intrinsic or extrinsic charge compensation? Quantitative charge analysis of PAH/PSS multilayers, Langmuir 18 (2002) 6694–6698, https://doi.org/10.1021/la020108n.

[38] M. Elzbieciak, S. Zapotoczny, P. Nowak, R. Krastev, M. Nowakowska, P. Warszynski, Influence of pH on the structure of multilayer films composed of strong and weak polyelectrolytes, Langmuir 25 (2009) 3255–3259, https://doi.org/10.1021/la803988k.

[39] T.R. Sinclair, D. Robles, B. Raza, S. van den Hengel, S.A. Rutjes, A.M.d.R. Husman, J. de Grooth, W.M. de Vos, H.D.W. Roesink, Virus reduction through microfiltration membranes modified with a cationic polymer for drinking water applications, Colloid. Surf. a-Physicochem. Eng. Asp. 551 (2018) 33–41, https://doi.org/10.1016/j.colsurfa.2018.04.056.

[40] N.K. Penta, P.R.D. Veera, S.V. Babu, Charge density and pH effects on polycation adsorption on poly-Si, SiO2, and Si3N4 films and impact on removal during chemical mechanical polishing, ACS Appl. Mater. Interface. 3 (2011) 4126–4132, https://doi.org/10.1021/am2010114.

[41] F. Petrakli, M. Arkas, A. Tsetsekou, alpha-Alumina nanospheres from nano-dispersed boehmite synthesized by a wet chemical route, J. Am. Ceram. Soc. 101 (2018) 3508–3519, https://doi.org/10.1111/jace.15487.

[42] S.M. Notley, Adsorption of polyelectrolyte modified graphene to silica surfaces: monolayers and multilayers, J. Colloid. Interface Sci. 375 (2012) 35–40, https://doi.org/10.1016/j.jcis.2012.02.060.

[43] A.C. Ferrari, D.M. Basko, Raman spectroscopy as a versatile tool for studying the properties of graphene, Nat. Nanotechnol. 8 (2013) 235–246, https://doi.org/10.1038/nnano.2013.46.

[44] L.G. Cancado, A. Jorio, E.H. Ferreira, F. Stavale, C.A. Achete, R.B. Capaz, M. V. Moutinho, A. Lombardo, T.S. Kulmala, A.C. Ferrari, Quantifying defects in graphene via Raman spectroscopy at different excitation energies, Nano Lett. 11 (2011) 3190–3196, https://doi.org/10.1021/nl201432g.

[45] S. Sanchez-Cortes, R.M. Berenguel, A. Madejon, M. Perez-Mendez, Adsorption of polyethyleneimine on silver nanoparticles and its interaction with a plasmid DNA: a surface-enhanced Raman scattering study, Biomacromolecules 3 (2002) 655–660, https://doi.org/10.1021/bm015640o.

[46] H. Xuan, W. Dai, Y. Zhu, J. Ren, J. Zhang, L. Ge, Self-Healing, antibacterial and sensing nanoparticle coating and its excellent optical applications, Sens. Actuat. B 257 (2018) 1110–1117, https://doi.org/10.1016/j.snb.2017.11.078.
[47] H. Xuan, J. Ren, J. Zhang, L. Ge, Novel highly-flexible, acid-resistant and self-healing host-guest transparent multilayer films, Appl. Surf. Sci. 411 (2017) 303–314, https://doi.org/10.1016/j.apsusc.2017.03.129.
[48] L. Feng, S.H. Li, Y.S. Li, H.J. Li, L.J. Zhang, J. Zhai, Y.L. Song, B.Q. Liu, L. Jiang, D. B. Zhu, Super-hydrophobic surfaces: from natural to artificial, Adv. Mater. 14 (2002) 1857–1860, https://doi.org/10.1002/adma.200290020.
[49] T.Y. Liu, C.J. Kim, Turning a surface superrepellent even to completely wetting liquids, Science 346 (2014) 1096–1100, https://doi.org/10.1126/science.1254787.
[50] M.J. Kreder, J. Alvarenga, P. Kim, J. Aizenberg, Design of anti-icing surfaces: smooth, textured or slippery? Nat. Rev. Mater. 1 (2016) https://doi.org/10.1038/natrevmats.2015.3.
[51] M. Humood, K. Polychronopoulou, Y. Song, J.C. Grunlan, A.A. Polycarpou, In situ nanomechanical behavior and self-healing response of polymeric multilayer thin films, Polymer (Guildf) 131 (2017) 169–178, https://doi.org/10.1016/j.polymer.2017.10.036.
[52] R. Saha, W.D. Nix, Effects of the substrate on the determination of thin film mechanical properties by nanoindentation, Acta Mater. 50 (2002) 23–38, https://doi.org/10.1016/s1359-6454(01)00328-7.

Supplementary Information

Water enabled self-healing polymeric coating with reduced graphene oxide-reinforcement for sensors

*Kally C.S. Ly [1,2], Mawin J.M. Jimenez[1], Silvia Cucatti[1], Diogo Volpati[3], Marcelo A. Pereira-da-Silva[4,5], Flavio M. Shimizu[6], Tiago P. Almeida[1,7], Varlei Rodrigues[1], Alberto F. da Silva[8], Fernando Alvarez[1], Antonio Riul Jr[1] *.*

[1] Department of Applied Physics, "*Gleb Wataghin*" Institute of Physics (IFGW), University of Campinas (UNICAMP), 13083-970, Campinas, SP, Brazil.

[2] School of Material Science and Engineering, Shanghai Jiao Tong University (SJTU), Shanghai, China.

[3] Sol Voltaics AB, 223 63, Lund, Sweden

[4] Instituto de Física de São Carlos – IFSC/USP, 13560-250, São Carlos, SP, Brazil.

[5] Centro Universitário Central Paulista - UNICEP, São Carlos, SP,Brasil

[6] Brazilian Nanotechnology National Laboratory (LNNano), Brazilian Center for Research in Energy and Materials (CNPEM), 13083-970, Campinas, SP, Brazil.

[7] Department of Biotechnology, Delft University of Technology, Van der Maasweg 9, 2629 HZ Delft, The Netherlands

[8] Department of Analytical Chemistry, Chemistry Institute, University of Campinas (UNICAMP), 13083-970, Campinas, SP, Brazil.

* Corresponding author: riul@ifi.unicamp.br

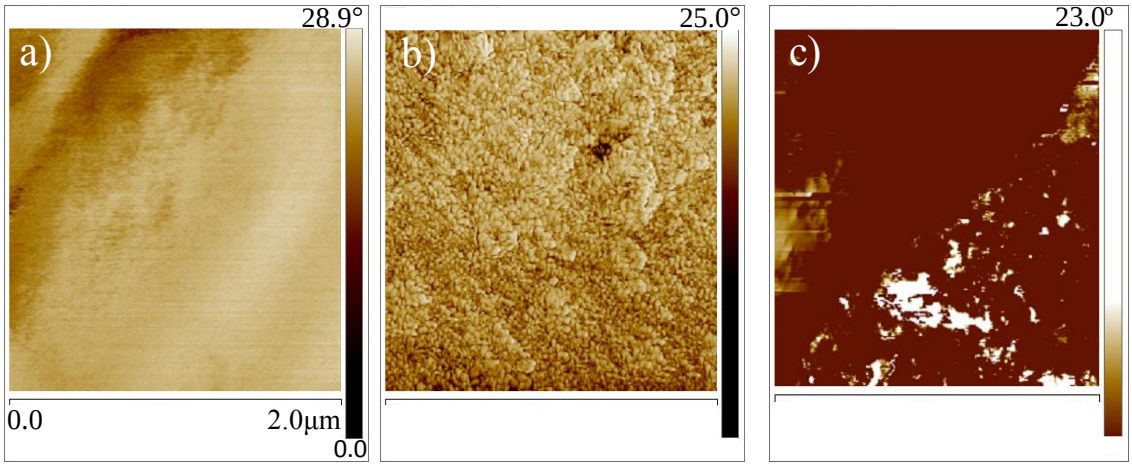

Fig. S1. AFM phase image of a) $(GPAH\text{-}PEI/GPSS\text{-}PAA)_{60}$, b) $(PEI/PAA)_{60}$ and c) $(GPAH/GPSS)_{50}$. By phase change, it is possible observe in a) the hybrid structure, while b) and c) are relatively homogeneous. All figures are at the same length scale.